Originally posted 27 October 2011; corrected 4 November 2011

www.sciencemag.org/cgi/content/full/science.1213782/DC1

Supporting Online Material for

Increasing the Potency and Breadth of an HIV Antibody by Using Structure-Based Rational Design

Ron Diskin, Johannes F. Scheid, Paola M. Marcovecchio, Anthony P. West, Jr., Florian Klein, Han Gao, Priyanthi N. P. Gnanapragasam, Alexander Abadir, Michael S. Seaman, Michel C. Nussenzweig, Pamela J. Bjorkman*

*To whom correspondence should be addressed. E-mail: bjorkman@caltech.edu

Published 27 October 2011 on *Science* Express
DOI: 10.1126/science.1213482

This PDF file includes:

Correction: The sequence alignment numbering in Fig. S1 was corrected.

Supporting Online Material for

Increasing the Potency and Breadth of an HIV Antibody using Structure-Based Rational Design

Ron Diskin[1], Johannes F. Scheid[2,3], Paola M. Marcovecchio[1], Anthony P. West, Jr. [1], Florian Klein[2], Han Gao[1], Priyanthi N. P. Gnanapragasam[1], Alexander Abadir[2], Michael S. Seaman[4], Michel C. Nussenzweig[2,5] and Pamela J. Bjorkman[1,6]

[1]Division of Biology and [6]Howard Hughes Medical Institute, California Institute of Technology, 1200 E. California Blvd., Pasadena, CA 91125

[2]Laboratory of Molecular Immunology and [5]Howard Hughes Medical Institute, The Rockefeller University, New York, NY 10065

[3]Charite Universitätsmedizin, D-10117 Berlin, Germany

[4]Beth Israel Deaconess Med. Ctr., Boston, MA 02215; United States

This PDF file includes

MATERIALS AND METHODS

Protein expression and purification

Proteins were produced and purified using previously-described methods (*34*). Briefly, NIH45-46 IgG was expressed by transient transfection in HEK293-6E cells. Secreted IgG was purified from cell supernatants using protein A affinity chromatography (GE Healthcare). Fab fragments were prepared by digesting purified IgG with immobilized papain (Pierce) at 10 mg/mL and then separating Fabs from Fc-containing proteins using protein A chromatography and Superdex 200 16/60 size exclusion chromatography. For crystallization trials, the NIH45-46 Fab for crystallization experiments was concentrated to 11 mg/mL in 20 mM Tris pH 8.0, 150 mM sodium chloride, 0.02% sodium azide (TBS). Substitutions in heavy chain residue 54 of NIH45-46, 3BNC55, 12A12, 3BNC117 and 3BNC60 were introduced using a Quikchange II kit (Agilent technologies). Wild type, mutant forms and chain swapped versions of these proteins were expressed as IgGs in HEK293-6E cells and purified by protein A chromatography as described for NIH45-46 IgG. Proteins were stored at a concentration of 1 mg/mL for neutralization assays in either 10 mM sodium citrate pH 3.05, 50 mM sodium chloride, 0.02% sodium azide or in TBS (12A12 and 12A12^{Y54W}) or in phosphate buffered saline (NIH45-46 mutated/truncated in CDRH3 and NIH45-46/VRC01 heavy and light chain swapped antibodies (Abs)) prior to dilution into neutral pH cell media. For SPR analyses, NIH45-46 and NIH45-46^{G54W} heavy chains were subcloned into the pTT5 (NRC-BRI) expression vector to encode C-terminal 6x-His tagged Fab heavy chains (V_H-C_H1–6x-His tag), and the heavy chain expression vectors were co-transfected with the appropriate light chain vector into HEK293-6E cells. Supernatants were collected after 7 days, buffer exchanged into TBS and loaded on a Ni^{2+}-NTA affinity column (Qiagen). Fabs were eluted using TBS supplemented with 250 mM imidazole and further purified by Superdex 200 10/300 size exclusion chromatography (GE Healthcare) in TBS.

Genes encoding truncated 93TH053, CAP244.2.00.D3, and Q259.d2.17 gp120 cores including the deletions and modifications described in ref. (*25*) were chemically synthesized (BlueHeron). An extra disulfide bond was introduced into 93TH053 by changing the Val65 and Ser115 codons into cysteines. The modified core genes were subcloned into the pACgp67b expression vector (BD Biosynthesis) to include a C-terminal 6x-His tag, expressed in baculovirus-infected insect cells, and purified from insect cell supernatants as previously described (*34*). For crystallization experiments, purified NIH45-46 Fab and 93TH057 gp120 were incubated at a 1:1 molar ratio and treated with 40 kU of Endoglycosidase H (New England Biolabs) for 16 hours at 37° C. The complex was purified after the incubation by Superdex 200 10/300 size exclusion chromatography (GE Healthcare) and then concentrated to OD_{280} = 9.6 in 20 mM Tris pH 8.0, 300 mM sodium chloride, 0.02% sodium azide.

Crystallization

Crystallization screening was done by vapor diffusion in sitting drops by a Mosquito® crystallization robot (TTP labs) using 400 nL drops (1:1 protein to reservoir ratio) utilizing commercially available crystallization screens (Hampton). Initial crystallization hits for Fab NIH45-46 and for NIH45-46–93TH057 complex were identified using the PEGRx HT™ (Hampton) screen and then manually optimized. Thin needle-like crystals of Fab NIH45-46 (space group $P2_12_12_1$, a = 49.4 Å, b = 87.4 Å, c = 166.4 Å; one molecule per asymmetric unit) were obtained upon mixing a

protein solution at 11 mg/mL with 12% polyethylene glycol 20,000, 0.1 M sodium acetate pH 5.0, 0.1 M sodium/potassium tartrate, 0.02 M ammonium sulfate at 20 °C. Crystals were briefly soaked in mother liquor solution supplemented with 15% and then 30% glycerol before flash cooling in liquid nitrogen. Crystals of the NIH45-46–93TH057 complex (space group $P2_12_12_1$, a = 69.1 Å, b = 70.5 Å, c = 217.7 Å; one molecule per asymmetric unit) were obtained upon mixing a protein solution at OD_{280}=9.6 with 12% isopropanol, 10% polyethylene glycol 10,000, 0.1 M sodium citrate pH 5.0 at 20 °C. Complex crystals were cryo-cooled by covering the crystallization drops with paraffin oil to prevent evaporation and then adding an excess of 20% isopropanol, 5% glycerol, 10% polyethylene glycol, 0.1 M sodium citrate pH 5.0 to the drops prior to mounting and flash cooling the crystals in liquid nitrogen.

Data collection, structure solution and refinement

X-ray diffraction data were collected at the Stanford Synchrotron Radiation Lightsource (SSRL) beamline 12-2 using a Pilatus 6M pixel detector (Dectris). The data were indexed, integrated and scaled using XDS (*35*). The Fab NIH45-46 structure was solved by molecular replacement using Phaser (*36*) and the V_HV_L and C_H1C_L domains of the VRC01 Fab (PDB code 3NGB) as separate search models. The model was refined to 2.6 Å resolution using an iterative approach involving refinement using the Phenix crystallography package (*37*) and manually fitting models into electron density maps using Coot (*38*). The final model (R_{work} = 18.4%; R_{free} = 23.8%) includes 3380 protein atoms, 125 water molecules and 37 ligand atoms, including N-Acetylglucosamine, glycerol and a sulfate ion (Table S1). 96.5%, 3.3% and 0.2% of the residues were in the favored, allowed and disallowed regions, respectively, of the Ramachandran plot. The first glutamine of the NIH45-46 heavy chain was modeled as 5-pyrrolidone-2-carboxylic acid.

A search model for solving the NIH45-46–93TH057 complex was created by superimposing the refined structure of the NIH45-46 Fab on the VRC01 Fab in the structure of VRC01–93TH057 (PDB code 3NGB). A molecular replacement solution was found as described above using separate search models for the V_HV_L domains of NIH45-46 complexed with 93TH057 and the C_H1C_L domains of NIH45-46. (Table S1). The complex structure was refined to 2.45 Å resolution as described for the Fab structure. To reduce model bias, the CDRH3 of NIH45-46 was omitted from the model and then built into electron density maps after a few rounds of refinement. Formation of an introduced disulfide bond between residues 65 and 115 in 93TH057 gp120 was verified in a Fo - Fc annealed omit electron density map contoured at 3.0 σ. The final model (R_{work} = 20.7%; R_{free} = 25.6%) includes 5989 protein atoms, 67 water molecules and 148 atoms of carbohydrates, citrate and chloride ions (Table S1). 96.1%, 3.5% and 0.4% of the residues were in the favored, allowed and disallowed regions, respectively, of the Ramachandran plot. Disordered residues that were not included in the model were residues 1-2 of the NIH45-46 light chain, residues 133-136 and 219-221 of the heavy chain, and residues 302-308 (V3 substitution), residues 397-408 (a total of 6 residues from V4) and the 6x-His tag of 93TH057. The first glutamine of the NIH45-46 heavy chain was modeled as 5-pyrrolidone-2-carboxylic acid.

Buried surface areas were calculated using AreaIMol in CCP4 (*39*) and a 1.4 Å probe. Superimposition calculations were done and molecular representations were generated using PyMol (*40*).

Surface Plasmon Resonance (SPR) measurements

The binding of gp120 core proteins to wild-type NIH45-46 Fab and to mutant (NIH45-46^{G54W}) Fab was compared using a Biacore T100 instrument (GE Healthcare). Purified NIH45-46 and NIH45-46^{G54W} Fabs were immobilized at coupling densities of 500 resonance units (RU) or 1500 RU on a CM5 sensor chip (Biacore) in 10 mM acetate pH 5.0 using primary amine coupling chemistry as described in the Biacore manual. One of the four flow cells on each sensor chip was mock-coupled using buffer to serve as a blank. Experiments were performed at 25˚C in 20 mM HEPES, pH 7.0, 150 mM sodium chloride and 0.005% (v/v) surfactant P20, and the sensor chips were regenerated using 10 mM glycine, pH 2.5. gp120 core proteins were injected in a two-fold dilution series at concentrations ranging from 500 nM to 31.2 nM at a flow rate of 70 µL/min. After subtracting the signal from the mock-coupled flow cell, kinetic data were globally fit to a 1:1 binding model (Biacore evaluation software) to derive on- and off-rate constants, which were used to calculate affinities as $K_D = k_d/k_a$.

***In vitro* neutralization assays**

A previously-described pseudovirus neutralization assay was used to compare the neutralization potencies of wild-type and mutant IgGs (*41*). Neutralization assays were performed either by the Collaboration for AIDS Vaccine Discovery (CAVD) core neutralization facility (Fig 4A, Tables S5, S6) or by our laboratory (Fig. S5C, S8, Tables S2, S8) using the same protocol (*41*). Briefly, pseudoviruses were generated in HEK293T cells by co-transfection of an Env-expressing vector and a replication-incompetent backbone plasmid. Neutralization was assessed by measuring the reduction in luciferase reporter gene expression in the presence of a potential inhibitor following a single round of pseudovirus infection in TZM-bl cells. Antibodies were pre-incubated with 250 infectious viral units in a three or four-fold dilution series for one hour at 37°C before adding 10,000 TZM-bl cells per well for a two-day incubation. Cells were then lysed and luciferase expression was measured using BrightGlo (Promega) and a Victor3 luminometer (PerkinElmer). Nonlinear regression analysis using the program Prism (GraphPad) was used to calculate the concentrations at which half-maximal inhibition was observed (IC_{50} values) as described (*42*). Samples were initially screened in duplicates. Reagents that showed enhanced activity were tested again as triplicates. Values for NIH45-46 and NIH45-46^{G54W} in Fig. S8A were obtained from three independent experiments. Similar IC_{50} values were obtained in two independent neutralization experiments using different dilution series.

SUPPLEMENTARY DISCUSSION

Comparison of Tyr74 in NIH45-46 and VRC01

The conformation of heavy chain residue Tyr74, a FWR3 residue that was substituted during somatic hypermutation (*16*), differs in the NIH45-46 and VRC01 structures. In NIH45-46–93TH057, the hydroxyl of $Tyr74_{NIH45\text{-}46}$ hydrogen bonds with the carbonyl oxygen of $Leu122_{gp120}$ in the bridging sheet (Fig. S4B). The $Tyr74_{NIH45\text{-}46}$ sidechain adopts a similar orientation in the structure of unbound NIH45-46 despite a slight mainchain displacement (Fig. 1A). By contrast, in VRC01–93TH057, the $Tyr74_{VRC01}$ sidechain is stabilized by $Gly8_{VRC01}$ of a crystallographic neighbor; rather than hydrogen bonding with $Leu122_{gp120}$, it approaches $Gly124_{gp120}$ (part of a recombinant insert replacing V1-V2) (PDB code: 3NGB). As $Tyr74_{VRC01}$ probably occupies space filled by the V1-V2 stem, the conformation of Tyr74 observed in NIH45-46–93TH057 is likely favored when interacting with spike trimers on a virion, implying that VRC01, like NIH45-46, targets the bridging sheet as part of its binding surface on gp120. However, the $Leu122_{gp120}$ region of the bridging sheet was eliminated from the resurfaced RSC3 gp120 due to a truncation beginning at residue 121 (*8*) (Fig. S6).

Comparison of NIH45-46 and VRC01 light chains

Contacts between the antibody light chain and gp120 are mostly conserved between the NIH45-46–93THO57 and VRC01–93THO57 structures with a notable exception: $Ser28_{NIH45\text{-}46\ LC}$ in CDRL1 replaces a solvent-exposed tyrosine ($Tyr28_{VRC01\ LC}$) that interacts with ordered N-linked carbohydrate attached to $Asn276_{93TH057}$. By contrast, the $Ser28_{NIH45\text{-}46\ LC}$ sidechain does not contact gp120 carbohydrates; instead it faces away from gp120, hydrogen bonding with $Arg64_{NIH45\text{-}46\ LC}$ (FWR3) and creating a 2.7 Å displacement of the mainchain Cα atoms (Fig. S5A). The $Ser28_{NIH45\text{-}46\ LC}$–$Arg64_{NIH45\text{-}46\ LC}$ interaction is maintained in unbound NIH45-46 (Fig. S5B). The position 28 substitution of serine for tyrosine largely accounts for the burial of more surface area in gp120's interaction with the VRC01 versus NIH45-46 light chain (681 $Å^2$ versus 395 $Å^2$ total buried surface area; 314 $Å^2$ versus 203 $Å^2$ buried surface area on the light chain) (Table S4). The larger contact area for the VRC01 light chain may account for the ability of VRC01, but not NIH45-46, to neutralize the clade C CAP45.2.00.G3 strain, given that the NIH45-46 heavy chain paired with the VRC01 light chain neutralizes this strain, whereas the VRC01 heavy chain paired with the NIH45-46 light chain does not (Table S10). However, the VRC01 light chain did not increase the potency of NIH45-46 against three other viral strains (Fig. S5C), suggesting that the Tyr28 interaction with gp120 carbohydrate is not obligatory.

Figure S1

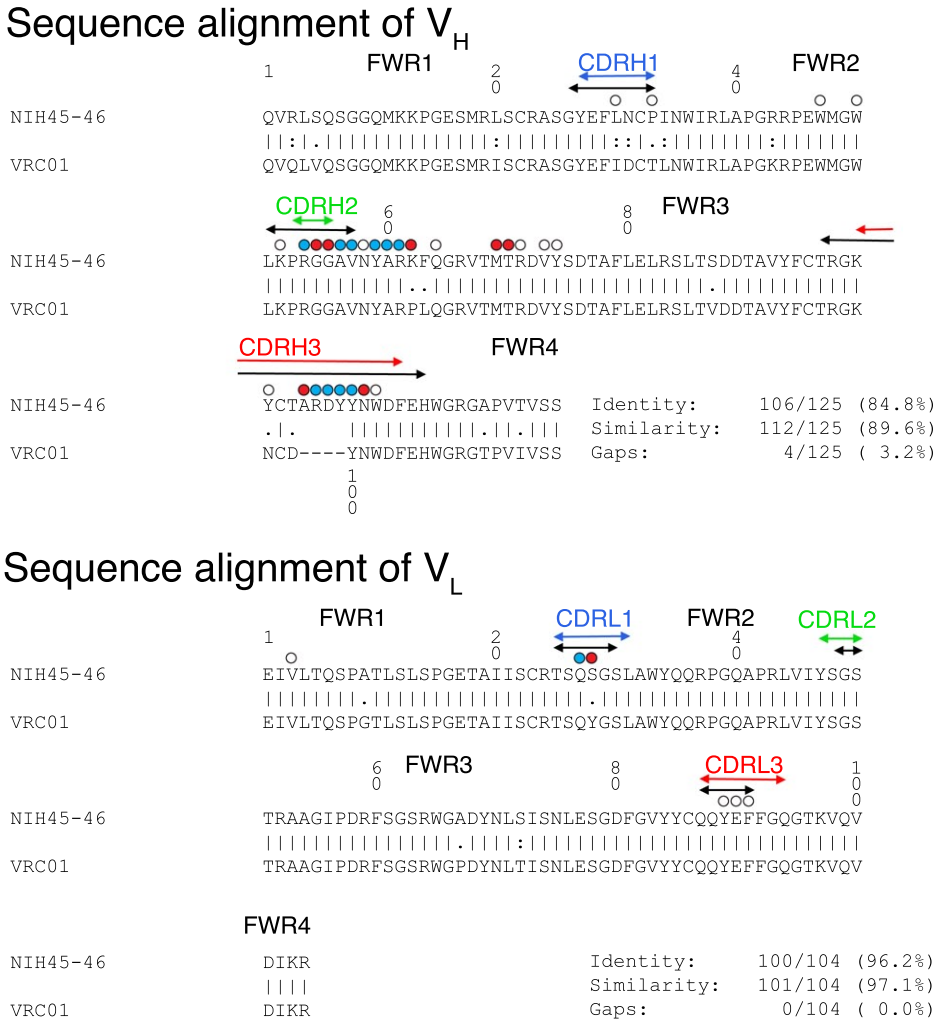

Fig. S1. Sequence alignment of NIH45-46 and VRC01 (residue are numbered as defined for VRC01 (*8*)). Circles mark NIH45-46 residues that contact gp120; unfilled circles indicate side chain contacts, red circles indicate main chain contacts, and blue circles indicate contacts with both the side and the main chain. Black arrows indicate the boundaries of complementarity determining regions (CDRs) as defined by IMGT (*43*), and residues within CDR loops as defined by the structure are marked with colors corresponding to the CDR colors in Fig. 1B. The locations of framework regions (FWRs) are indicated before, after, and between the CDRs. The definition of CDR2 in ref. (*8*) was the same as that defined by IMGT; however CDR2 was defined differently in refs. (*25, 26*) to include C-terminal residues within the C" β-strand and FWR3.

Figure S2

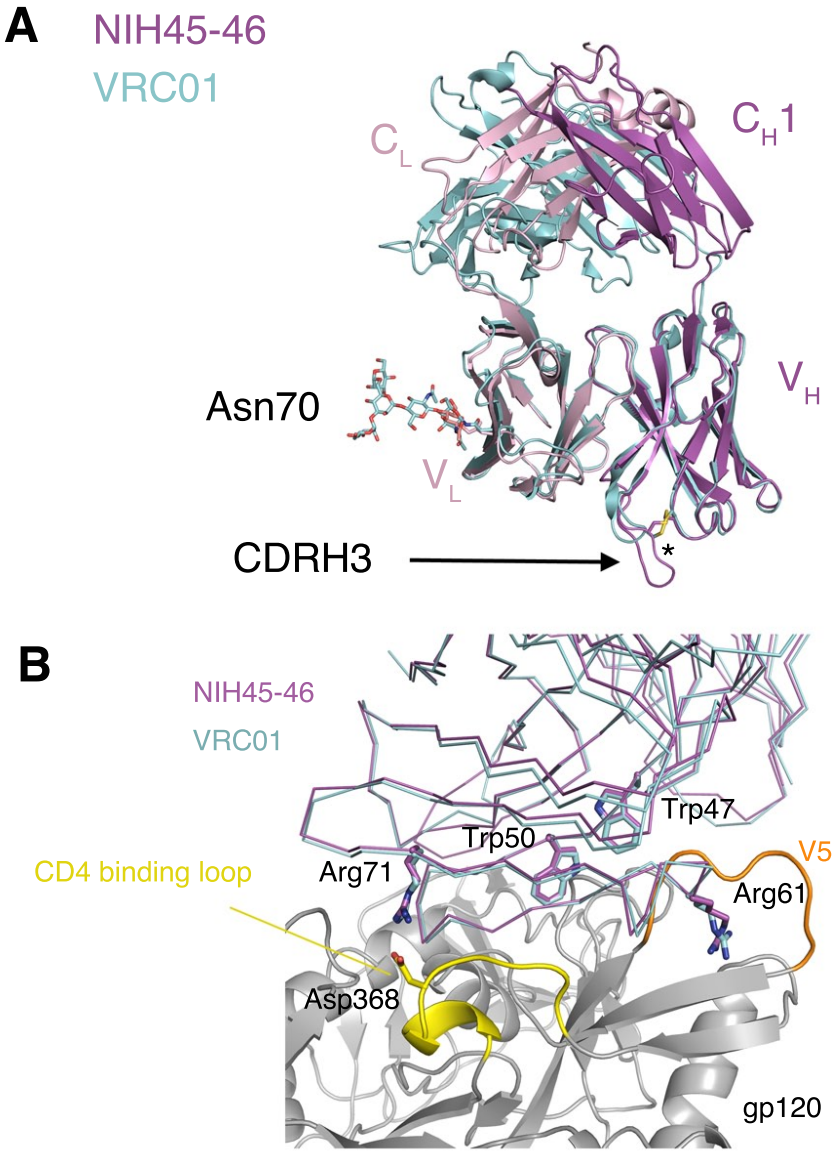

Fig. S2. Comparisons of NIH45-46 and VRC01 from the gp120-bound structures. (**A**) NIH45-46 in shown in magenta (heavy chain) and pink (light chain) and VRC01 is cyan. The additional disulfide bond joining CDRH2 and CDRH3 is indicated by an asterisk and carbohydrate attached to Asn70 is shown as sticks. An arrow points to CDRH3, which includes a four-residue insertion in NIH45-46. **(B)** Conserved interactions in the gp120 contacts of NIH45-46 and VRC01. The antigen-binding regions of the NIH45-46 (magenta) and VRC01 (cyan) Fabs are shown complexed with 93TH053 gp120 (gray with yellow CD4-binding loop and orange V5 loop). Contact residues that are conserved in both structures as sticks.

Figure S3

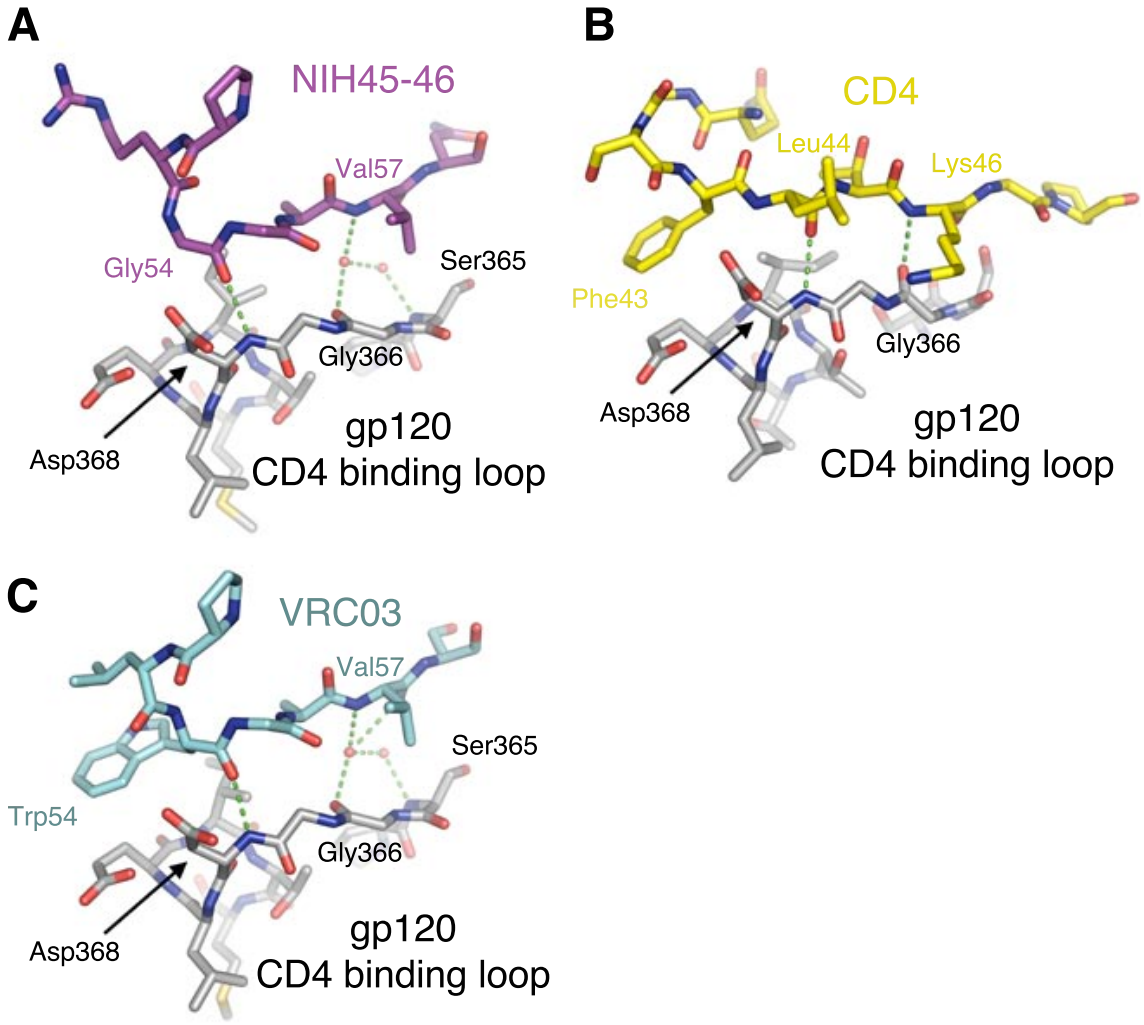

Fig. S3. Hydrogen bonding within the gp120 CD4-binding loop. (**A**) A direct hydrogen bond (green dotted line) forms between main chain atoms of $Gly54_{NIH45-46}$ (magenta) and $Asp368_{gp120}$ (gray), and two water molecules (red spheres) mediate a hydrogen bond network between NIH45-46 and the CD4-binding loop. (**B**) CD4 (yellow) forms two direct hydrogen bonds with the CD4-binding loop (*31*). (**C**) The carbonyl oxygen of $Trp54_{VRC03}$ (cyan) forms a direct hydrogen bond with $Asp368_{gp120}$ (PDB code: 3SE8) using a similar architecture as shown for NIH45-46 in panel A, demonstrating that a tryptophan can be accommodated at position 54 without disrupting the hydrogen bond to $Asp368_{gp120}$.

Figure S4

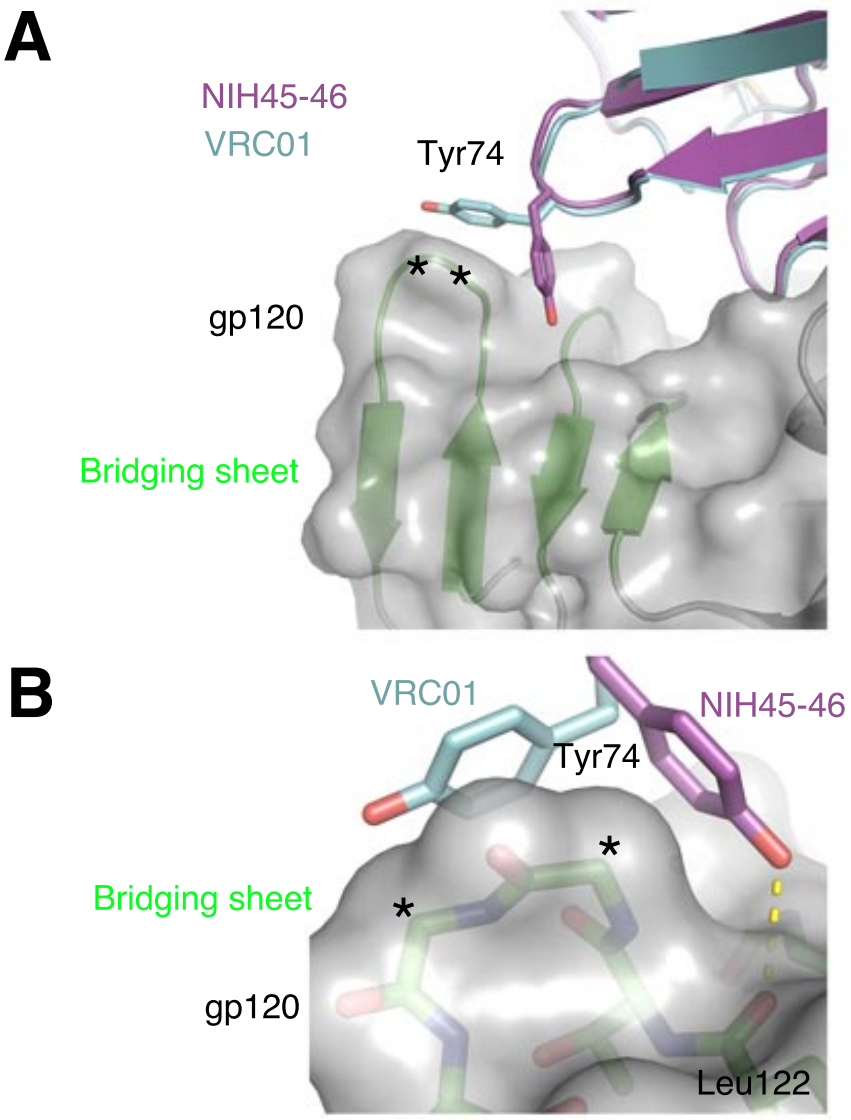

Fig. S4. Conformation of $Tyr74_{NIH45-46}$ (see Supplementary Discussion). (**A**) Superimposition of NIH45-46 (magenta) and VRC01 (cyan) in the bound states shows different conformations of heavy chain residue Tyr74. The gp120 bridging sheet is green and asterisks indicate the recombinant Gly_2 linker that replaces the V1-V2 loop. (**B**) Close-up showing the hydrogen bond between $Tyr74_{NIH45-46}$ and the main chain carbonyl oxygen of $Leu122_{gp120}$.

Figure S5

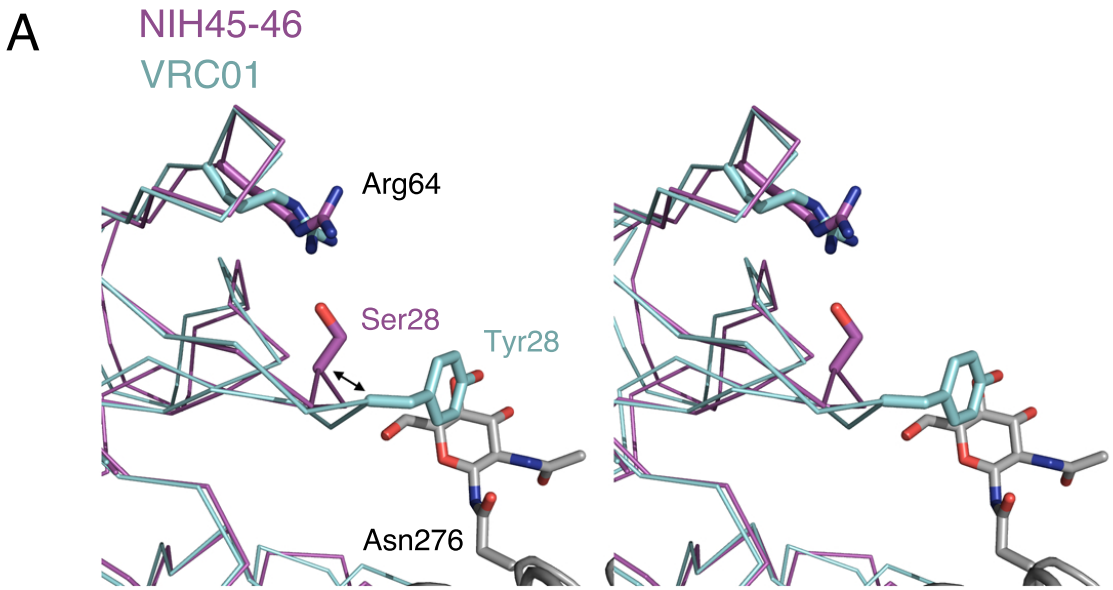

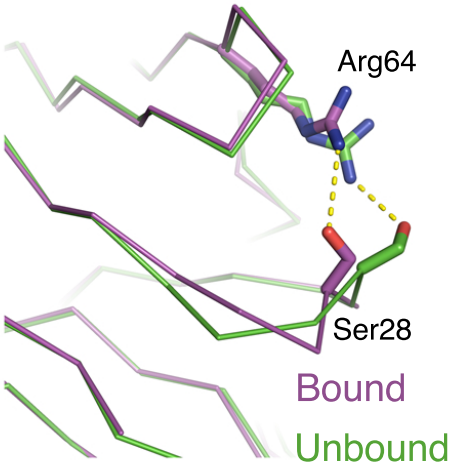

C

***In vitro* neutralization IC_{50} values (μg/mL)**

Virus	Clade	NIH45-46	NIH45-46 HC VRC01 LC	VRC01 HC NIH45-46 LC	VRC01
AC10.0.29	B	0.9	1.0	4.5	0.8
TRO.11	B	1.9	0.3	24	0.5
SC422661.8	B	0.05	0.2	0.4	0.2
QH0692.42	B	0.7	0.9	1.2	0.7
ZM214M.PL15.11	C	0.5	0.6	1.8	0.8
CAP45.2.00.G3	C	>50	2.1	>50	1.8
T257-31	CRF02 (A/G)	0.5	0.6	15	1.0

Fig. S5. The NIH45-46 light chain (see Supplementary Discussion). (**A**) Stereo view of the superimposition of NIH45-46 and VRC01 light chains (magenta and cyan, respectively). $Tyr28_{VRC01\ LC}$ interacts with N-linked carbohydrate attached to $Asn276_{gp120}$. By contrast, the side chain of the counterpart residue in NIH45-46, $Ser28_{NIH45\text{-}46\ LC}$, faces away from gp120 to hydrogen bond with $Arg64_{NIH45\text{-}46\ LC}$, which results in a 2.7 Å local displacement of the NIH45-46 main chain relative to VRC01 (arrowheads point to Ca atoms of residue 28 in each structure). (**B**) Superimposition of $NIH45\text{-}46_{light\ chain}$ in the bound and unbound structures (magenta and green, respectively) showing hydrogen bonds between Ser28 and Arg64. (**C**) Comparisons of neutralization by wild-type versus light chain-swapped antibodies. Color-coded according to IC_{50} values (μg/mL): red <0.1, orange 0.1-1, yellow 1-10, green 10-50, white > 50 (not neutralizing).

Figure S6

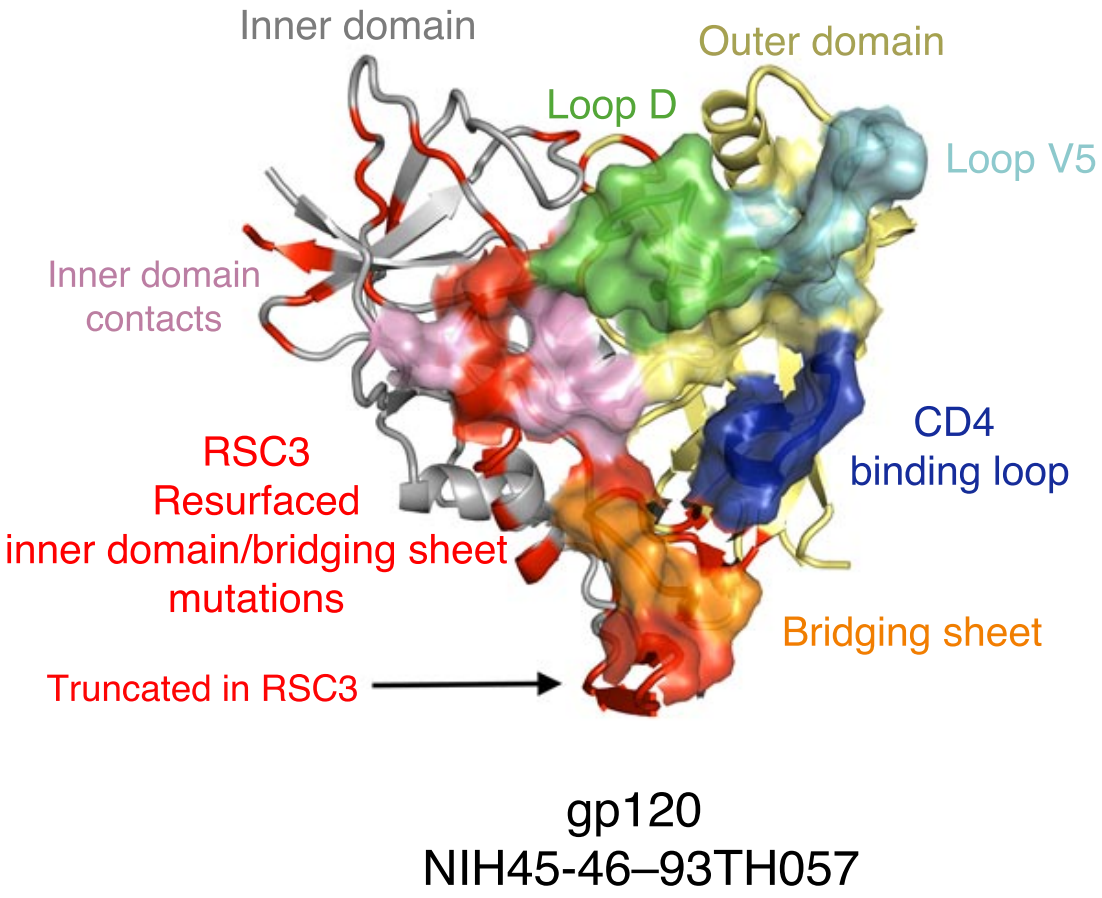

Fig. S6. NIH45-46 contact surfaces that were mutated in RSC3. 93TH057 gp120 is shown using a ribbon diagram and color coded as in Fig. 1B. Residues at each contact interface are highlighted on the gp120 structure as a surface enclosing the contact residues. The surface area on the inner domain that is buried by contact with NIH45-46 is shown in pink with inner domain/bridging sheet residues that were mutated in RSC3 (*8*) in red.

Figure S7

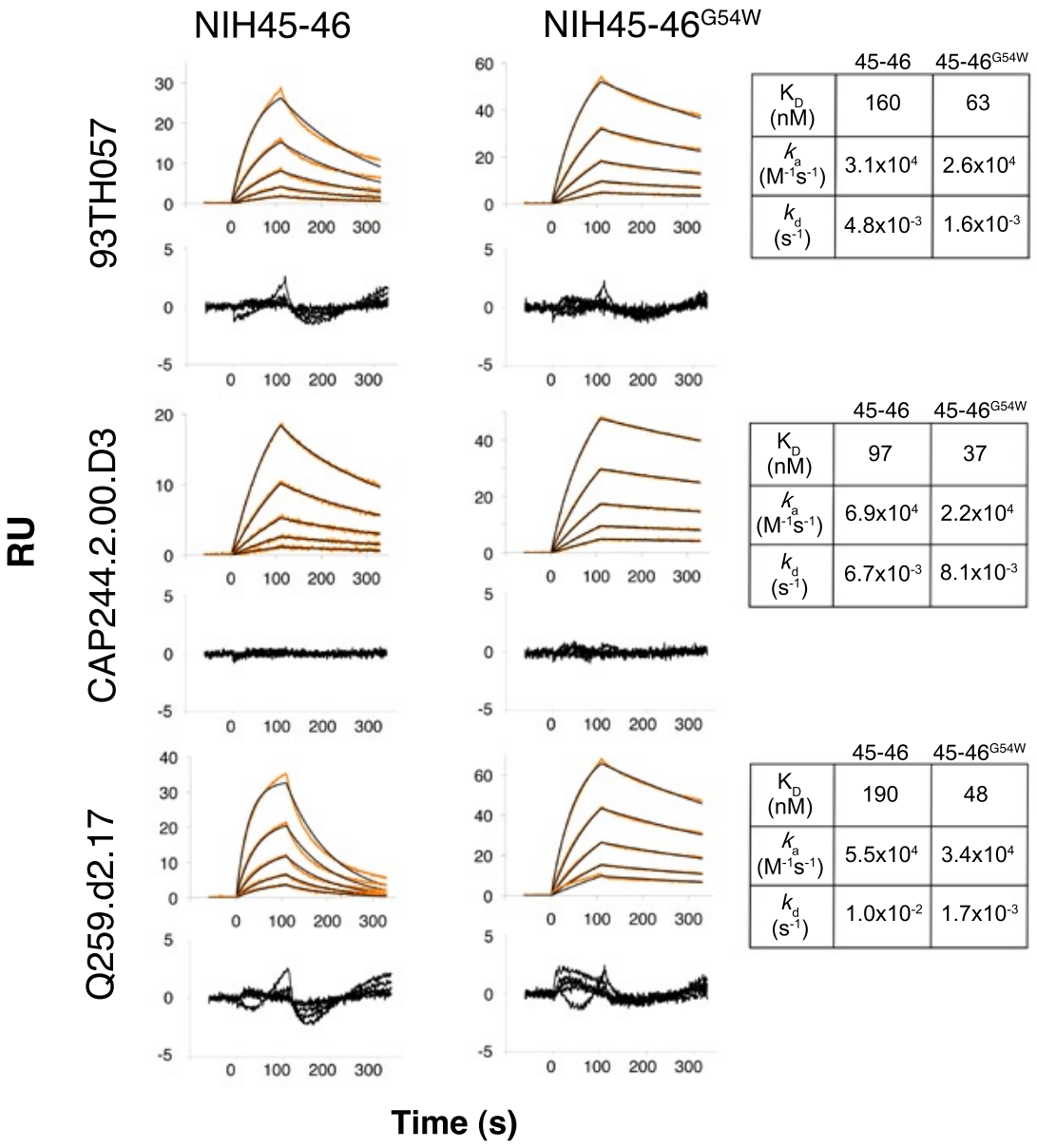

Fig. S7. Sensorgrams from SPR experiments comparing the binding of the indicated gp120 core proteins to NIH45-46 or NIH45-46^{G54W} Fabs. The gp120 proteins were injected as a concentration series (500 nM to 31.2 nM; two-fold dilutions) over Fabs that were immobilized at a surface density of 1500 RU. (Similar results were obtained in independent experiments in which the IgGs were immobilized at 500 RU; data not shown). Best-fit binding curves (black lines) for a 1:1 binding model are superimposed on the raw data (orange). Corresponding residual plots are shown below each sensorgram.

Figure S8

A

Virus	Clade	NIH45-46 IC_{50} (μg/mL)							
		WT	G54W	G54F	G54Y	G54I	G54M	G54L	G54H
SC422661.8	B	0.06	0.03	0.02	0.06	0.1	0.06	0.1	0.09
AC10.0.29	B	0.9	0.2	0.3	0.4	8.6	1.5	1.7	0.6
TRO.11	B	1.0	0.09	0.08	0.1	10	0.3	0.3	0.2
Du172.17	C	>50	0.9	16	>50	>50	>50	>50	>50
CAP210.2.00.E8	C	>50	41	>50	>50	>50	>50	>50	>50
CAP45.2.00.G3	C	>50	6.6	>50	45	>50	>50	>50	>50

B

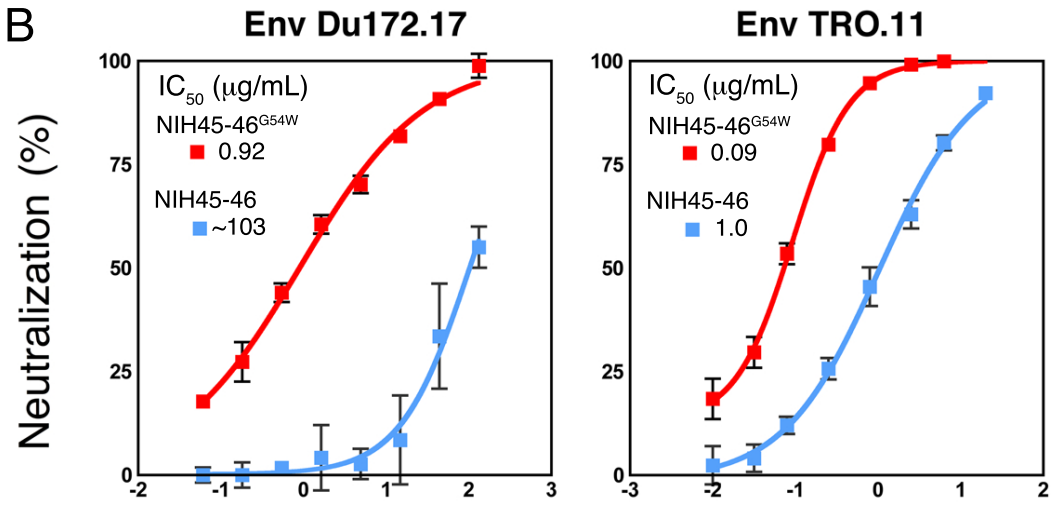

Fig. S8. Increased neutralization potency of NIH45-46^{G54W}. (**A**) *In vitro* neutralization data for a panel of six viruses chosen to include NIH45-46–sensitive and resistant strains color-coded according to IC_{50} values (μg/ml): red <0.1, orange 0.1-1, yellow 1-10, green 10-50, white >50 (not neutralizing). (**B**) Representative neutralization curves showing the activity of NIH45-46^{G54W} (red) and NIH45-46 (cyan). The experimental points are averaged values from three independent assays. Error bars indicate standard deviations. The IC_{50} value for NIH45-46 against strain DU172.17 was extrapolated from data that do not reach saturation in assays conducted with high concentrations to detect weak neutralizing activity.

Table S1

Data collection and refinement statistics

	NIH45-46–93TH057	Fab NIH45-46
Data collection		
Wavelength (Å)	0.953	0.953
Space group	$P2_12_12_1$	$P2_12_12_1$
Cell dimensions		
a, *b*, *c* (Å)	69.1, 70.5, 217.7	49.4, 87.4, 166.4
α, β, γ (°)	90.0, 90.0, 90.0	90.0, 90.0, 90.0
Resolution (Å)	37.05-2.45 (2.51-2.45)	38.68-2.60 (2.67-2.60)
R_{meas} (%)	7.5 (66.9)	12.2 (105.6)
$R_{mrgd\text{-}F}$ (%)	11.6 (108.1)	13.1 (78.0)
$I / \sigma I$	10.8 (1.8)	12.83 (2.0)
Completeness (%)	98.6 (98.7)	99.5 (99.9)
Multiplicity	3.7	6.6
Reflections	145342	150105
Unique reflections	39062	22795
Refinement		
Resolution (Å)	37.05-2.45	38.68-2.6
No. reflections	38987	22692
R_{work} / R_{free}	20.7 / 25.6	18.4 / 23.8
No. atoms		
Protein	5989	3380
Ligand/ion	148	37
Water	67	125
B-factors		
Protein	79.9	46.0
Ligand/ion	106.4	80.9
Water	62	42.0
Ramachandran		
Favored (%)	96.12	96.49
Allowed (%)	3.48	3.28
Outlier (%)	0.40	0.23
R.m.s. deviations		
Bond lengths (Å)	0.004	0.004
Bond angles (°)	0.754	0.838

5% of unique reflections were removed as a test set for the R_{free} calculation.

Values in parentheses are for the highest resolution shell.

Table S2

Effects of the insertion in NIH45-46 on neutralization potency

In vitro neutralization IC_{50} values (µg/mL)

Virus	Clade	NIH45-46 WT	NIH45-46 Y99dA	NIH45-46 Δ99a-99d
AC10.0.29	B	0.9	4.4	13
TRO.11	B	1.9	>50	>50
SC422661.8	B	0.05	0.08	1.4
QH0692.42	B	0.7	2.1	3.7
ZM214M.PL15.11	C	0.3	1.1	2.2
CAP45.2.00.G3	C	>50	>50	>50
T257-31	CRF02 (A/G)	0.5	2.4	7.0

	CDRH3 sequence
NIH45-46 WT	FCTRGKYCTARDYYNWDFEHWGRGAP
NIH45-46 Y99dA	FCTRGKYCTARDAYNWDFEHWGRGAP
NIH45-46 Δ99a-99d	FCTRGKYCT----YNWDFEHWGRGAP

Color-coded according to IC_{50} values (µg/mL): red <0.1, orange 0.1-1, yellow 1-10, green 10-50, white > 50 (not neutralizing). IC_{50} values for VRC01 tested against the same viral strains are shown in Fig. S5C.

Table S3

Comparison of *in vitro* neutralization data for viral strains with differences at residue 281

Strain	Sequence	Residue 281_{gp120}	IC_{50}* µg/mL
Du156.12	QLLLNGSLAEEEIIIKSENLTDN**I**KTIIVQLNQSIGINCTRPNNNTRKSV	I	0.01
ZM197M.PB7	QLLLNGSLAEEEIIIRSENLTDN**T**KTIIVHLNESVEIECVRPNNNTRKSV	T	0.14
ZM214M.PL15	QLLLNGSLAEKEIMIRSENLTNN**A**KTIIVQLTEAVNITCMRPGNNTRRSV	A	0.05
ZM249M.PL1	QLLLNGSLAEKEIIIRSENITDN**V**KIIIVHLNESVEINCTRPNNNTRKSI	V	0.02
ZM53M.PB12	QLLLNGSTAEEDIIIRSENLTNN**A**KTIIVHLNESIEIECTRPGNNTRKSI	A	0.65
ZM109F.PB4	QLLLNGSLAEEEIVIRSENLTDN**A**KTIIVHLNKSVEIECIRPGNNTRKSI	A	0.22
ZM135M.PL10a	QLLLNGSLSEEGIIIRSKNLTDN**T**KTIIVHLNESVAIVCTRPNNNTRKSI	T	0.36

* IC_{50} values for NIH45-46 are taken from ref. (*16*).

Table S4

Buried Surface Area (Å^2)

	FWR1	CDR1	FWR2	CDR2	FWR3	CDR3	Total Fab	Interface on gp120	CDR2 + FWR3$_{56-65}$*
NIH45-46 HC	0	35	51	181	551	326	**1144**	**1097**	576
VRC01 HC	0	20	98	136	521	117	**892**	**882**	545
NIH45-46 LC	35	8	0	0	0	159	**203**	**192**	0
VRC01 LC	36	114	0	0	0	165	**314**	**367**	0

*Box on the right with blue numbering: Residues that correspond to the CDR2 region as defined in ref. (*25*).

	Inner domain & bridging sheet	Loop D + NAG	β-15/α-3 + NAG	V5	β-24	Outer domain exit loop	Total gp120	Interface on Fab or CD4
NIH45-46	328	335	222	292	81	35	**1290**	**1346**
VRC01	157	433	208	328	43	57	**1225**	**1206**
CD4	400	136	263	155	14	97	**973**	**1059**

<10%
10-20%
20-30%
30-40%
40-50%
>50%

Table S4. Buried surface areas were calculated using Areaimol in CCP4 (*44*). Color coding indicates the percent of the total buried surface area for each molecule. The insertion in CDRH3 contributes to a higher total buried surface area between the NIH45-46 heavy chain and gp120 compared with VRC01 (2241 Å^2 versus 1774 Å^2 total buried surface area; 1144 Å^2 versus 892 Å^2 buried surface area on the heavy chain). The difference in heavy chain buried area is largely due to more extensive gp120 contacts of the CDRH3$_{NIH45-46}$ loop: 326 Å^2 of surface area of the NIH45-46 CDRH3 are buried by contacting gp120, compared with 117 Å^2 for the VRC01 CDRH3. The extra contacts with gp120 created by the CDRH3 insertion allow the NIH45-46 footprint on gp120 to more closely resemble the CD4 footprint on gp120 than does the VRC01 footprint (Fig. 3C). In particular, CD4 makes at least 1/3 of its contacts with the inner domain and bridging sheet of gp120, as opposed to only 13% of the total surface area contacted by VRC01 involving non-outer domain elements of gp120 (*25*). The contact area with the inner domain and bridging sheet is increased to 25% in the NIH45-46 footprint on gp120.

Table S5

In vitro neutralization IC_{50} values (µg/mL)

			NIH45-46 IC_{50} (µg/mL)			
Virus	**Clade**	**Category**	**WT**	**G54W**	**G54F**	**G54Y**
6545.v4.c1	AC	R	>50	18.92	>50	>50
6540.v4.c1	AC	R	>50	>50	>50	>50
CAP45.2.00.G3	C	R	>50	32.25	>50	>50
Du422.1	C	R	>50	>50	>50	>50
CAP210.2.00.E8	C	R	>50	>50	>50	>50
3817.v2.c59	CD	R	>50	>50	>50	>50
89-F1_2_25	CD	R	>50	>50	>50	>50
620345.c01	CRF01_AE	R	>50	>50	>50	>50
T250-4	CRF02_AG	R	>50	1.33	>50	>50
T278-50	CRF02_AG	R	>50	>50	>50	>50
211-9	CRF02_AG	R	>50	16.41	>50	>50
3016.v5.c45	D	R	>50	1.47	5.82	17.89
Du172.17	C	R	>50	3.65	>50	>50
3718.v3.c11	A	P	19.61	0.01	0.32	0.30
703357.C02	CRF01_AE	P	19.17	3.43	7.91	5.60
CNE20	BC	P	7.83	0.04	0.53	0.33
CNE21	BC	P	6.01	0.03	0.12	0.07
HIV-16845-2.22	C	P	5.00	0.45	0.59	0.59
C2101.c01	CRF01_AE	P	4.24	0.04	0.11	0.09
ZM247v1(Rev-)	C	P, T/F	2.94	0.32	0.28	0.42
ZM233M.PB6	C	P	2.50	0.02	0.22	0.16
C1080.c03	CRF01_AE	P	2.48	0.20	0.36	0.29
THRO4156.18	B	P	1.91	0.54	0.89	0.66
3103.v3.c10	ACD	P	1.770	0.200	0.370	0.300
231966.c02	D	P	1.640	0.020	0.060	0.060
TRO.11	B	P	1.610	0.040	0.110	0.080
T251-18	CRF02_AG	P	1.350	0.260	0.410	0.350
Ce1176_A3	C	S, T/F	0.930	0.160	0.240	0.210
QH0692.42	B	S	0.720	0.370	0.560	0.520
T255-34	CRF02_AG	S	0.710	<0.001	0.030	0.040
ZM135M.PL10a	C	S	0.590	0.040	0.130	0.090
AC10.0.29	B	S	0.560	0.130	0.240	0.190
T257-31	CRF02_AG	S	0.490	0.130	0.170	0.180
CNE58	BC	S	0.430	0.020	0.040	0.040
Ce0393_C3	C	S, T/F	0.334	0.013	0.040	0.036
R1166.c01	CRF01_AE	S	0.310	0.130	0.400	0.240
CNE30	BC	S	0.309	0.052	0.100	0.099
CNE17	BC	S	0.261	0.036	0.075	0.073
X2131_C1_B5	G	S	0.230	0.050	0.100	0.100
928-28	CRF02_AG	S	0.230	0.060	0.110	0.120
6535.3	B	S	0.230	0.030	0.070	0.080

Virus	Clade	Category	WT	G54W	G54F	G54Y
ZM53M.PB12	C	S	0.175	0.040	0.080	0.060
ZM214M.PL15	C	S	0.170	0.030	0.090	0.060
Ce703010054_2A2	C	S, T/F	0.159	0.027	0.020	0.022
ZM197M.PB7	C	S	0.150	0.040	0.090	0.070
CAAN5342.A2	B	S	0.150	0.070	0.100	0.100
Q23.17	A	S	0.140	0.010	0.030	0.020
PVO.4	B	S	0.120	0.050	0.070	0.060
1054_07_TC4_1499	B	S, T/F	0.113	0.040	0.076	0.064
Ce2010_F5	C	S, T/F	0.101	0.038	0.046	0.049
ZM109F.PB4	C	S	0.095	0.002	0.022	0.026
1056_10_TA11_1826	B	S, T/F	0.094	0.024	0.064	0.044
0330.v4.c3	A	S	0.090	0.030	0.040	0.030
P1981_C5_3	G	S	0.080	0.020	0.030	0.040
Q461.e2	A	S	0.076	0.009	0.030	0.023
P0402_c2_11	G	S	0.073	0.003	0.008	0.012
SC422661.8	B	S	0.060	0.020	0.040	0.040
62357_14_D3_4589	B	S, T/F	0.060	0.020	0.040	0.030
WITO4160.33	B	S	0.060	0.010	0.020	0.030
Ce2060_G9	C	S, T/F	0.058	0.005	0.022	0.021
Ce0682_E4	C	S, T/F	0.054	0.010	0.011	0.017
231965.c01	D	S	0.051	<0.001	0.022	0.025
Q259.d2.17	A	S	0.043	<0.001	0.009	0.009
TRJO4551.58	B	S	0.040	0.010	0.030	0.030
6811.v7.c18	CD	S	0.035	<0.001	0.017	0.011
R2184.c04	CRF01_AE	S	0.034	0.005	0.015	0.015
6480.v4.c25	CD	S	0.032	0.004	0.014	0.018
X1254_c3	G	S	0.032	0.002	0.011	0.013
Q842.d12	A	S	0.031	0.005	0.011	0.015
C3347.c11	CRF01_AE	S	0.029	<0.001	0.015	0.011
1006_11_C3_1601	B	S, T/F	0.027	<0.001	0.003	0.005
3415.v1.c1	A	S	0.022	<0.001	<0.001	<0.001
X1193_c1	G	S	0.021	<0.001	<0.001	0.006
Du156.12	C	S	0.020	<0.001	<0.001	0.007
RHPA4259.7	B	S	0.017	<0.001	0.005	0.007
ZM249M.PL1	C	S	0.017	0.002	0.004	0.003
0815.v3.c3	ACD	S	0.014	<0.001	<0.001	<0.001
REJO4541.67	B	S	0.014	0.002	0.007	0.007
3301.v1.c24	AC	S	0.009	<0.001	0.001	0.003
Q769.d22	A	S	0.009	<0.001	0.005	0.007
CNE53	BC	S	0.008	<0.001	0.005	0.006
WEAU_d15_410_787	B	S, T/F	0.005	<0.001	<0.001	0.002
Geometric means			**0.417**	**0.046**	**0.120**	**0.124**

Category R - Resistant S - Sensitive
P - Poorly sensitive T/F - Transmitted Founder

IC_{50} values (µg/mL) color coding	<0.01	0.01-0.1	0.1-1.0	1.0-10	10-50	>50

Table S6

In vitro neutralization IC_{80} values (µg/mL)

			NIH45-46 IC_{80} (µg/mL)			
Virus	**Clade**	**Category**	**WT**	**G54W**	**G54F**	**G54Y**
T250-4	CRF02_AG	R	>50	**44.94**	>50	>50
703357.C02	CRF01_AE	R	>50	**17.61**	>50	**30.58**
CAP45.2.00.G3	C	R	>50	>50	>50	>50
CNE20	BC	R	>50	**0.48**	**3.91**	**2.40**
CAP210.2.00.E8	C	R	>50	>50	>50	>50
T278-50	CRF02_AG	R	>50	>50	>50	>50
211-9	CRF02_AG	R	>50	>50	>50	>50
620345.c01	CRF01_AE	R	>50	>50	>50	>50
3016.v5.c45	D	R	>50	**15.37**	**36.97**	>50
3817.v2.c59	CD	R	>50	>50	>50	>50
89-F1_2_25	CD	R	>50	>50	>50	>50
6540.v4.c1	AC	R	>50	>50	>50	>50
6545.v4.c1	AC	R	>50	>50	>50	>50
Du422.1	C	P	>50	>50	>50	>50
3718.v3.c11	A	P	>50	**0.04**	**4.620**	**3.85**
Du172.17	C	P	>50	**42.85**	>50	>50
CNE21	BC	P	**38.07**	**0.16**	**0.66**	**0.29**
C2101.c01	CRF01_AE	P	**31.37**	**0.17**	**0.42**	**0.27**
ZM247v1(Rev-)	C	P, T/F	**24.50**	**2.60**	**2.45**	**3.57**
HIV-16845-2.22	C	P	**22.61**	**2.10**	**2.75**	**2.75**
ZM233M.PB6	C	P	**14.18**	**0.11**	**0.99**	**0.78**
C1080.c03	CRF01_AE	P	**11.56**	**0.91**	**2.26**	**1.83**
231966.c02	D	P	**9.64**	**0.11**	**0.24**	**0.23**
THRO4156.18	B	P	**8.22**	**1.81**	**3.01**	**2.14**
TRO.11	B	P	**7.49**	**0.13**	**0.30**	**0.22**
3103.v3.c10	ACD	P	**6.15**	**0.56**	**1.28**	**0.81**
T251-18	CRF02_AG	P	**3.68**	**0.92**	**1.38**	**1.16**
T255-34	CRF02_AG	S	**3.442**	**0.099**	**0.198**	**0.174**
Ce1176_A3	C	S, T/F	**3.17**	**0.45**	**0.83**	**0.58**
ZM135M.PL10a	C	S	**2.79**	**0.16**	**0.43**	**0.30**
CNE58	BC	S	**2.08**	**0.05**	**0.11**	**0.11**
AC10.0.29	B	S	**1.93**	**0.63**	**1.12**	**0.90**
QH0692.42	B	S	**1.71**	**1.12**	**1.65**	**1.50**
T257-31	CRF02_AG	S	**1.38**	**0.45**	**0.51**	**0.67**
R1166.c01	CRF01_AE	S	**1.21**	**0.51**	**1.32**	**0.84**
CNE30	BC	S	**1.067**	**0.196**	**0.348**	**0.263**
Ce0393_C3	C	S, T/F	**0.936**	**0.089**	**0.173**	**0.134**
X2131_C1_B5	G	S	**0.88**	**0.24**	**0.41**	**0.39**
CNE17	BC	S	**0.734**	**0.127**	**0.287**	**0.264**
928-28	CRF02_AG	S	**0.64**	**0.25**	**0.41**	**0.33**

Virus	Clade	Category	WT	G54W	G54F	G54Y
ZM53M.PB12	C	S	0.61	0.16	0.23	0.22
ZM214M.PL15	C	S	0.59	0.15	0.30	0.23
ZM197M.PB7	C	S	0.55	0.18	0.23	0.21
6535.3	B	S	0.54	0.13	0.27	0.24
Ce703010054_2A2	C	S, T/F	0.538	0.077	0.070	0.070
Q23.17	A	S	0.50	0.03	0.07	0.06
1056_10_TA11_1826	B	S, T/F	0.447	0.160	0.283	0.189
ZM109F.PB4	C	S	0.437	0.070	0.17	0.168
PVO.4	B	S	0.41	0.16	0.25	0.18
1054_07_TC4_1499	B	S, T/F	0.404	0.165	0.283	0.236
CAAN5342.A2	B	S	0.40	0.21	0.28	0.27
Ce2010_F5	C	S, T/F	0.357	0.187	0.186	0.235
0330.v4.c3	A	S	0.3	0.11	0.13	0.09
Q461.e2	A	S	0.291	0.091	0.135	0.103
Ce2060_G9	C	S, T/F	0.290	0.042	0.085	0.068
WITO4160.33	B	S	0.26	0.04	0.14	0.09
P1981_C5_3	G	S	0.24	0.07	0.11	0.09
P0402_c2_11	G	S	0.214	0.023	0.047	0.049
1006_11_C3_1601	B	S, T/F	0.196	0.008	0.024	0.021
62357_14_D3_4589	B	S, T/F	0.19	0.07	0.14	0.09
Ce0682_E4	C	S, T/F	0.155	0.039	0.056	0.065
Q259.d2.17	A	S	0.154	0.014	0.036	0.034
SC422661.8	B	S	0.13	0.07	0.10	0.09
TRJO4551.58	B	S	0.13	0.05	0.08	0.07
R2184.c04	CRF01_AE	S	0.127	0.036	0.054	0.045
231965.c01	D	S	0.126	0.035	0.062	0.054
6811.v7.c18	CD	S	0.113	0.033	0.063	0.059
X1254_c3	G	S	0.107	0.018	0.043	0.041
6480.v4.c25	CD	S	0.100	0.021	0.046	0.051
C3347.c11	CRF01_AE	S	0.094	0.028	0.059	0.052
3415.v1.c1	A	S	0.086	0.023	0.029	0.037
Q842.d12	A	S	0.073	0.025	0.039	0.045
X1193_c1	G	S	0.064	0.009	0.026	0.024
Du156.12	C	S	0.054	0.005	0.019	0.026
ZM249M.PL1	C	S	0.053	0.007	0.016	0.011
0815.v3.c3	ACD	S	0.052	0.003	0.014	0.015
RHPA4259.7	B	S	0.047	0.007	0.020	0.020
CNE53	BC	S	0.039	0.005	0.024	0.027
REJO4541.67	B	S	0.035	0.013	0.028	0.020
3301.v1.c24	AC	S	0.033	0.004	0.011	0.014
Q769.d22	A	S	0.033	0.009	0.023	0.024
WEAU_d15_410_787	B	S, T/F	0.015	0.003	0.004	0.008
Geometric means			**1.231**	**0.225**	**0.437**	**0.393**

Category R - Resistant S - Sensitive
P - Poorly sensitive T/F - Transmitted Founder

IC_{80} values (µg/mL) color coding	<0.01	0.01-0.1	0.1-1.0	1.0-10	10-50	>50

Table S7

Sequence correlates of resistance to NIH45-46

Strain	gp120 residue variations that may affect NIH45-46 neutralization		
620345_c1	Ser456 (Arg)	Asp459 (Gly)	Lys279 (Asn/Asp)
89_F1_2_25	Ser456 (Arg)	Asn458 (Gly)	
6540_v4_c1	Ser456 (Arg)	Tyr458 (Gly)	Ser280 (Asn)
6545_v4_c1	Ser456 (Arg)	Tyr458 (Gly)	Ser280 (Asn)
Du422.1	Trp456 (Arg)		
T250_4	Pro459 (Gly)		
T278_50	Glu459 (Gly)	Ala279 (Asn/Asp)	
Ce1172_H1	deletion of Gly459		
X2088_c9	Val459 (Gly)		
H086.8	Asp459 (Gly)	Lys279 (Asn/Asp)	

Table S7. 10 of 17 NIH45-46–resistant strains (5 of 7 NIH45-46^{G54W}–resistant strains, shown in bold) have amino acid variations at NIH45-46-contacting residues that have a fully conserved residue (shown in parenthesis) in all NIH45-46 sensitive strains. These mutations occur in the β23 strand immediately preceding V5 and in loop D. The positions of shaded sites have been shown to be important in resistance to VRC01 (*33*).

For the remaining strains, resistance may relate to other features:

Strain	Possible NIH45-46 resistance correlate
Du172.17	Lys462 (positive residue unusual at this position)
3016.v5.c45	Tyr282 (Lys) (likely a steric issue – change in loop D conformation); neutralized by VRC01
CAP45.2.00.G3	VRC01 light chain permits neutralization ($Tyr28_{VRC01\ LC}$-glycan at $Asn276_{gp120}$)
3817.v2.c59	Quaternary effect suggested in ref. (*33*)
CAP210.2.00.E8	Mechanism unclear
246F C1G	
211-9	

The largest difference between sensitivity to NIH45-46 and sensitivity to VRC01 was in strain 3016.v5.c45 (IC_{50}s of >30 and 0.16 μg/mL, respectively). The most notable residue in 3016.v5.c45 is Tyr282 in loop D. This large residue may alter the conformation of loop D, which is closely contacted by the four-residue insertion in the NIH45-46 CDRH3. The absence of the insertion may permit VRC01 to better accommodate an altered loop D. The next largest NIH45-46/VRC01 difference, for strain C2101.c1 (12.78 vs. 0.36 μg/mL), may similarly relate to the unusual $Lys99_{gp120}$ residue replacing the asparagine that favorably interacts with $Arg99b_{NIH45-46}$ in the NIH45-46–gp120 crystal structure.

Table S8

Effects of position 54 substitution in selected bNAbs

In vitro neutralization IC_{50} values (µg/mL)

Virus	Clade	3BNC60 WT	3BNC60 T54W	3BNC117 WT	3BNC117 T54W	3BNC55 WT	3BNC55 T54W	12A12 WT	12A12 Y54W
SC422661.8	B	0.1	0.1	0.07	0.07	0.3	0.6	0.2	0.2
AC10.0.29	B	13	3.1	6.5	2.8	>50	>50	0.6	0.5
TRO.11	B	0.07	0.06	0.6	0.6	7.6	>50	0.3	0.2
Du172.17	C	0.05	0.04	0.04	0.9	2	>50	0.2	0.1
CAP210.2.00.E8	C	4.7	5.0	11	2.8	>50	>50	>50	>50
CAP45.2.00.G3	C	10	19	16	23	>50	>50	0.4	0.2

Color-coded according to IC_{50} values (µg/mL): red <0.1, orange 0.1-1, yellow 1-10, green 10-50, white > 50 (not neutralizing).

Table S9

Potencies of currently-available bNAbs

IC_{50}

	Isolate	PGT-121	PGT-122	PGT-123	PGT-125	PGT-126	PGT-127	PGT-128	PGT-130	PGT-131	PGT-135	PGT-136	PGT-137	PGT-141	PGT-142	PGT-143	PGT-144	PGT-145	VRC01	VRC-PG04	PG9
Include >50 (µg/mL)	Geometric mean	0.53	1.03	0.66	1.85	1.05	2.92	0.39	3.07	7.27	9.53	30.39	23.53	3.15	2.40	3.14	13.62	0.91	0.45	0.57	1.27
	Arithmetic mean	16.63	19.39	18.29	25.81	21.75	26.19	15.31	25.39	31.06	34.91	44.02	41.22	24.62	23.30	24.62	33.76	12.83	4.41	7.92	15.89
	Median	0.31	2.02	0.35	34.97	1.08	42.83	0.10	22.98	50.00	50.00	50.00	50.00	16.01	9.46	13.76	50.00	0.86	0.34	0.30	0.62
Exclude >50 (µg/mL)	Geometric mean	0.07	0.13	0.08	0.09	0.08	0.17	0.06	0.24	0.41	0.32	2.25	1.68	0.33	0.24	0.34	1.58	0.30	0.32	0.30	0.36
	Arithmetic mean	2.17	3.21	2.44	3.34	2.82	2.39	1.56	3.09	2.80	3.88	12.74	10.51	3.80	2.99	4.32	6.87	2.59	1.04	1.99	4.33
	Median	0.03	0.05	0.03	0.04	0.04	0.08	0.02	0.16	0.52	0.17	7.81	3.46	0.35	0.21	0.31	2.06	0.29	0.32	0.20	0.23
	% viruses <50 (µg/mL)	70%	65%	67%	52%	60%	50%	72%	52%	40%	33%	16%	22%	55%	57%	56%	38%	78%	92%	88%	75%

Table S9. Potencies of currently-available bNAbs. **(A)** Comparison of mean and median IC_{50} (µg/mL) values for PGT antibodies and VRC01. A direct comparison between NIH45-46 and the PGT antibodies is not available. However VRC01 (which was shown in a direct comparison to be less potent than NIH45-46 (*16*)) was directly compared to the PGT antibodies using the same virus panel (*18*) and thus can serve as a reference for comparing NIH45-46 to the PGT antibodies. Mean IC_{50} values were calculated using data taken from ref. (*18*). Geometric and arithmetic means were calculated to include data for all viral strains (listed as Include >50, in which case, values reported as IC_{50} >50 µg/mL were entered as 50 µg/mL in the calculation) and to exclude viral strains in which the IC_{50} was >50 µg/mL (listed as Exclude >50, in which case the percent of viral strains with IC_{50}s < 50 µg/mL is also reported). Mean IC_{50}s are compared with the median IC_{50}s as reported in ref. (*18*). The table is color-coded according to IC_{50} values (µg/mL): red <0.1, orange 0.1-1, yellow 1-10, green 10-50, white >50 (not neutralizing) or the percent of viral strains neutralized: red >90, orange 80-90, yellow 70-80, green 50-70, white <50.

References and Notes

1. A. S. Fauci *et al.*, *Science* **321**, 530 (Jul 25, 2008).
2. M. J. McElrath, B. F. Haynes, *Immunity* **33**, 542 (Oct 29, 2010).
3. G. B. Karlsson Hedestam *et al.*, *Nat Rev Microbiol* **6**, 143 (Feb, 2008).
4. A. J. McMichael, P. Borrow, G. D. Tomaras, N. Goonetilleke, B. F. Haynes, *Nat Rev Immunol* **10**, 11 (Jan, 2010).
5. S. Zolla Pazner, T. Cardozo, *Nature reviews. Immunology* **10**, 527 (2010).
6. L. M. Walker *et al.*, *Science* **326**, 285 (Sep 3, 2009).
7. J. F. Scheid *et al.*, *Nature* **458**, 636 (Apr 2, 2009).
8. X. Wu *et al.*, *Science* **329**, 856 (Aug 13, 2010).
9. L. Stamatatos, L. Morris, D. R. Burton, J. R. Mascola, *Nat Med* **15**, 866 (Aug, 2009).
10. E. S. Gray *et al.*, *J Virol* **85**, 4828 (May, 2011).
11. I. Mikell *et al.*, *PLoS Pathog* **7**, e1001251 (2011).
12. A. Trkola *et al.*, *Nat Med* **11**, 615 (Jun, 2005).
13. J. R. Mascola *et al.*, *Nat Med* **6**, 207 (Feb, 2000).
14. A. J. Hessell *et al.*, *PLoS Pathog* **5**, e1000433 (May, 2009).
15. A. J. Hessell *et al.*, *Nature* **449**, 101 (Sep 6, 2007).
16. J. F. Scheid *et al.*, *Science* **333**, 1633 (Aug 11, 2011).
17. J. F. Scheid *et al.*, *J Immunol Methods* **343**, 65 (Apr 15, 2009).
18. L. M. Walker *et al.*, *Nature* **477**, 466 (Aug 17, 2011).
19. D. Corti *et al.*, *PLoS One* **5**, e8805 (2010).
20. M. Bonsignori *et al.*, *J Virol*, (Jul 27, 2011).
21. Q. J. Sattentau, R. A. Weiss, *Cell* **52**, 631 (Mar 11, 1988).
22. M. Thali *et al.*, *J Virol* **67**, 3978 (Jul, 1993).
23. B. Chen *et al.*, *Nature* **433**, 834 (Feb 24, 2005).
24. J. M. Decker *et al.*, *J Exp Med* **201**, 1407 (May 2, 2005).
25. T. Zhou *et al.*, *Science* **329**, 811 (Aug 13, 2010).
26. X. Wu *et al.*, *Science* **333**, 1593 (Aug 11, 2011).
27. Materials and methods are available as supporting material on Science Online.
28. G. Nabel, P. Kwong, J. Mascola, *Philosophical transactions - Royal Society. Biological sciences* **366**, 2759 (2011).
29. P. D. Kwong *et al.*, *Nature* **393**, 648 (Jun 18, 1998).
30. N. Madani *et al.*, *Structure* **16**, 1689 (Nov 12, 2008).
31. Taken from a crystal structure of Fab 21c plus CD4 domains 1 and 2 bound to the ZM135M.PL10a gp120 core at 2.45Å (to be submitted to the PDB).
32. Geometric mean IC_{50} calculations were done without excluding resistant strains by entering values of 50 µg/mL for strains with IC_{50} values >50 µg/mL.
33. Y. Li *et al.*, *J Virol* **85**, 8954 (Sep, 2011).
34. R. Diskin, P. M. Marcovecchio, P. J. Bjorkman, *Nat Struct Mol Biol* **17**, 608 (May, 2010).
35. W. Kabsch, *Acta Crystallogr D Biol Crystallogr* **66**, 125 (Feb, 2010).
36. A. J. McCoy *et al.*, *J. Appl. Cryst.* **40**, 658 (2007).
37. P. D. Adams *et al.*, *Acta Crystallogr D Biol Crystallogr* **66**, 213 (Feb, 2010).
38. P. Emsley, K. Cowtan, *Acta Crystallogr D Biol Crystallogr* **60**, 2126 (Dec, 2004).
39. Collaborative Computational Project Number 4, *Acta Crystallographica Section D-Biological Crystallography* **50**, 760 (1994).

40. L. Schrödinger. (The PyMOL Molecular Graphics System, 2011).
41. D. C. Montefiori, *Current protocols in immunology / edited by John E. Coligan ... [et al* **Chapter 12**, Unit 12 11 (Jan, 2005).
42. J. S. Klein *et al.*, *Proc Natl Acad Sci USA* **106**, 7385 (May 5, 2009).
43. M. P. Lefranc *et al.*, *Nucleic Acids Res* **37**, D1006 (Jan, 2009).
44. CCP4, *Acta Crystallogr.* **D50**, 760 (1994).